Studying Desert Dust from the Sahara and the Middle East using the Cyprus Atmospheric Remote Sensing Observatory over Limassol, Cyprus

A. Savva[1,2], A. Nisantzi[1,2], M. Poutli[1,2], C. Chrysostomou[1,2], G. Kotsias[1], F. Scarlatti[1], A. Lopatin[3], D. Hadjimitsis[1,2], A. Ansmann[4] and R.E. Mamouri[1,2]

[1]Eratosthenes Centre of Excellence, Limassol, 3012, Cyprus; [2]Department of Civil Engineering & Geomatics, Cyprus University of Technology, Limassol, 3036, Cyprus; [3]GRASP SAS, Villeneuve-d'Ascq, 59650, France; [4]Leibniz Institute for Tropospheric Research, 04318 Leipzig, Germany

Contact Author: athina.savva@eratosthenes.org.cy

Introduction

The Eastern Mediterranean, particularly Cyprus, is influenced by the transport of air masses from the Sahara Desert and the Arabian Peninsula. Many studies have shown that some optical and microphysical characteristics of these two aerosol types differ.

The main objective of the present study is to investigate the optical and the microphysical characteristics of desert dust from both regions with the synergy of Polarization Polly^{XT} Raman Lidar and the Cimel sun/sky photometer.

The analysis is performed utilizing the Generalized Retrieval of Atmosphere and Surface Properties (GRASP) algorithm. GRASP is a highly flexible inversion algorithm applicable in a variety of domains, including observations from both active and passive remote sensing methods. The algorithm is based on the general principles of numerical inversion and atmospheric radiation modelling. Lopatin et al. (2013, 2021) first proposed the application of the GRASP algorithm, utilizing the synergy between multi-wavelength Lidar and the Aerosol Robotic Network (AERONET) sun/sky photometer observations.

Methodology & Data

Aerosol observations from the Polly^{XT} Polarization Raman Lidar and the CUT-TEPAK AERONET (Aerosol Robotic NETwork) sun/sky photometer of the Cyprus Atmospheric Remote Sensing Observatory National facility (CARO NF) of ERATOSTHENES Centre of Excellence provide the vertical aerosol characteristics to the algorithm, while the sun photometer provides constraints on the quantity and type of aerosol.

Saharan and Arabian Dust-dominated cases were analyzed with GRASP algorithm and compared with measurements from the instruments.

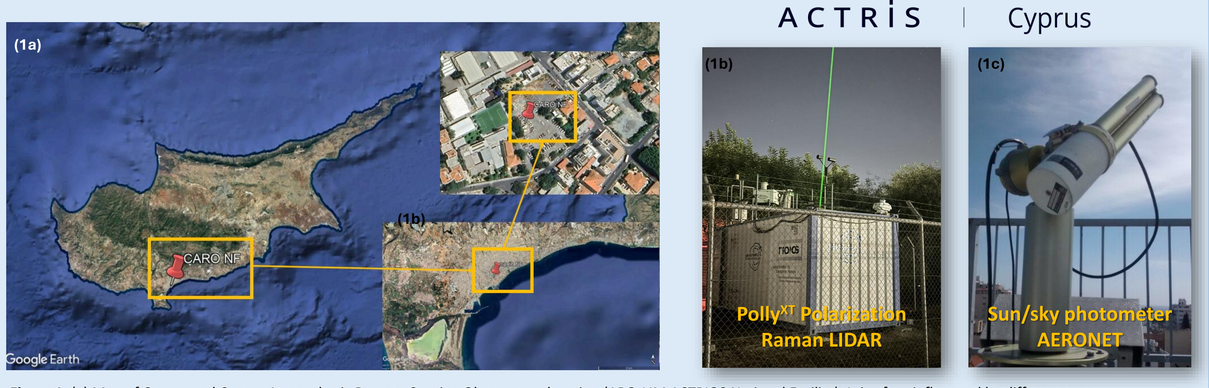

Figure 1. (a) Map of Cyprus and Cyprus Atmospheric Remote Sensing Observatory location (ARO-LIM ACTRIOS National Facility). It is often influenced by different type aerosol transportation from distant and neighboring regions . (b) Polly^{XT} Polarization Raman Lidar of ERATOSTHENES Centre of Excellence and (c) CUT-TEPAK AERONET sun/sky photometer of Cyprus University of Technology in Cyprus.

INPUT

Polly^{XT} Raman Lidar

(a) Elastic backscatter signals at 355, 532, 1064 nm,

(b) Volume Depolarization Ratio at 355, 532 nm.

Sun Photometer

(a) Total optical depths,

(b) Total scatter radiances at 340, 380, 440, 500, 675, 870, 1020 & 1064 nm.

→ **GRASP** →

OUTPUT

Aerosol properties (Fine & Coarse modes):

(a) Columnar properties

Size distribution, complex refractive index, single scattering albedo

(b) Vertical properties

Aerosol optical depth, single scattering albedo - (fine, coarse)

(c) Backscatter and extinction profiles.

Figure 2: Input and output of the GRASP algorithm.

Results

Saharan DUST Case
25 May 2025

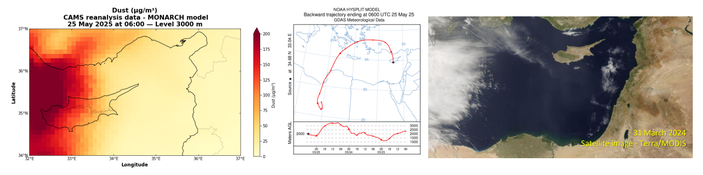

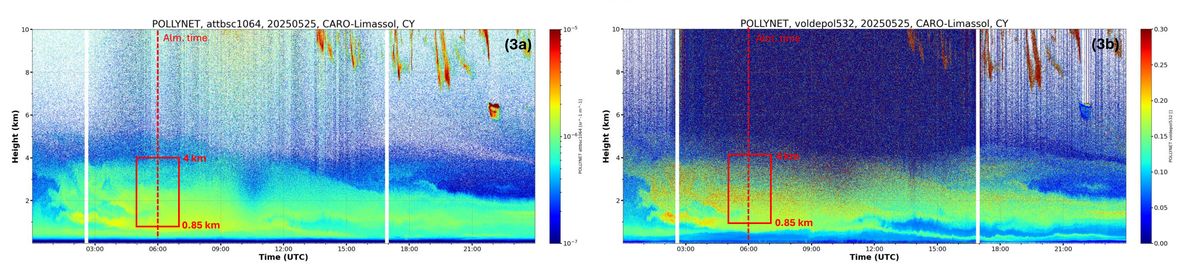

Figure 3: PollyXT lidar (a) Attenuated backscatter at 1064 nm (b) Volume linear depolarization ratio at 532 nm over Limassol, Cyprus, on 25 May 2025. Red boarders indicate the region of the studied aerosol layer and dashed line the almucantar studied time.

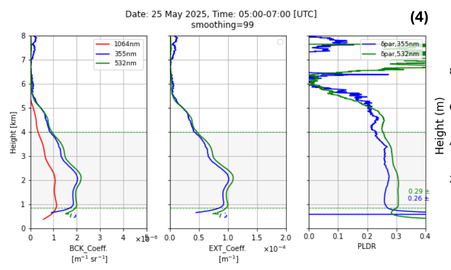

Figure 4: Vertical profiles of the backscatter coefficient, extinction coefficient, on particle depolarization ratio measured in Limassol, Cyprus 25 May 2025 from 05:00-07:00 UTC.

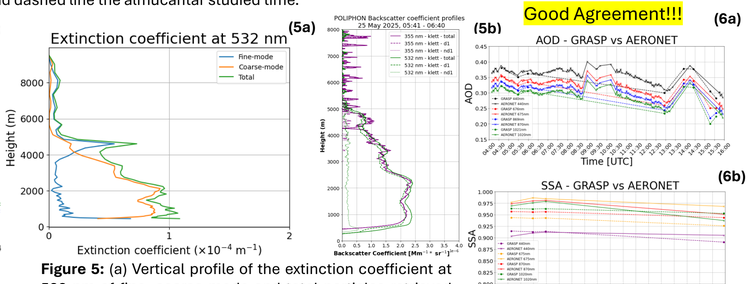

Figure 5: (a) Vertical profile of the extinction coefficient at 532 nm of fine, coarse mode and total particles retrieved using GRASP algorithm, (b) One-step POLIPHON vertical profiles of Klett backscatter coefficient for total at 355, 532, 1064 nm, dust and non-dust aerosol components.

Arabian DUST Case
31 March 2024

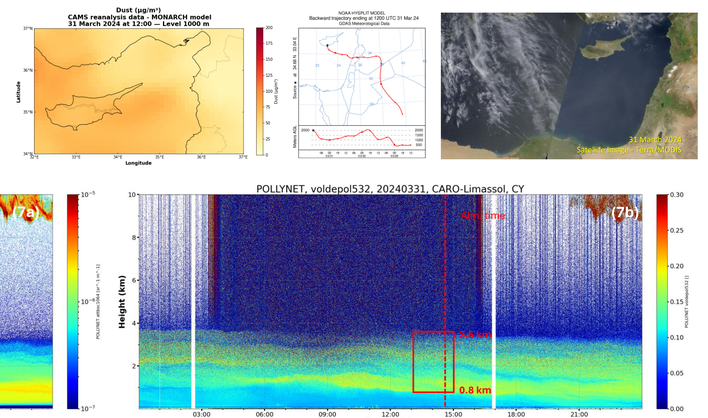

Figure 7: Polly^{XT} lidar (a) Attenuated backscatter at 1064 nm (b) Volume linear depolarization ratio at 532 nm over Limassol, Cyprus, on 31 March 2024. Red boarders indicate the region of the studied aerosol layer and dashed line the almucantar studied time.

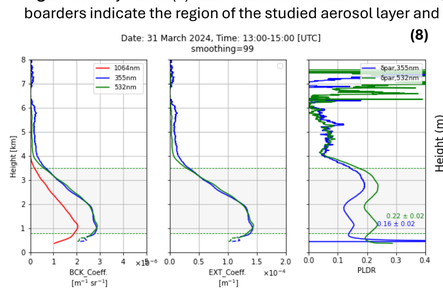

Figure 8: Vertical profiles of the backscatter coefficient, extinction coefficient, particle depolarization ratio measured in Limassol, Cyprus on 31 March 2024 from 13:00-15:00 UTC.

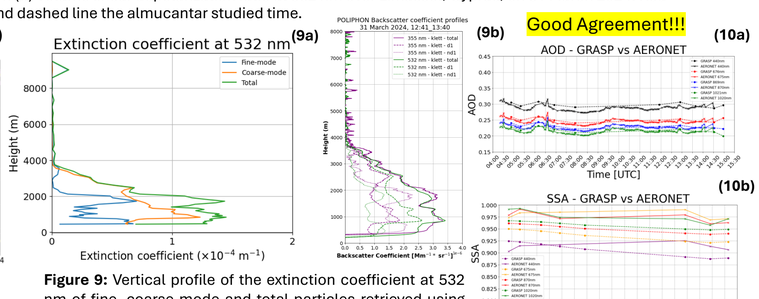

Figure 9: Vertical profile of the extinction coefficient at 532 nm of fine, coarse mode and total particles retrieved using GRASP algorithm, (b) One-step POLIPHON vertical profiles of Klett backscatter coefficient for total at 355, 532, 1064 nm, dust and non-dust aerosol components.

Layer information

			Geo info	Optic info								Micro info		
Case	Time (UTC)	Almucantar time	Layer height (km)	$\delta_{355\ nm}$ [%] (Klett LIDAR)	$\delta_{532\ nm}$ [%] (Klett LIDAR)	$S_{355\ nm}$ (sr)* (Raman LIDAR)	$S_{532\ nm}$ (sr)* (Raman LIDAR)	$AOD_{532\ nm}$ (LIDAR)	$AOD_{532\ nm}$ (GRASP)	AOD_F 532 nm (GRASP)	AOD_C 532 nm (GRASP)	SSA_F 440 nm (GRASP)	SSA_C 440 nm (GRASP)	SSA 440 nm (GRASP)
Saharan	05:00 - 07:00	05:58:32	0.85 - 4	0.26 ± 0.01	0.29 ± 0.02	49.36 ± 9.45	44.85 ± 5.61	0.274	0.237	0.024	0.212	0.756	0.982	0.951
Arabian	13:00 - 15:00	12:55:08	0.8 - 3.5	0.16 ± 0.02	0.22 ± 0.02	61.33 ± 6.95	56.82 ± 10.03	0.281	0.223	0.55	0.168	0.738	0.984	0.904

Columnar information

			Geo info	Optic info			Micro info							
Case	Almucantar time		Height	$AOD_{440\ nm}$ (GRASP)	$AOD_{440\ nm}$ (AERONET)	$AE_{440\text{-}870\ nm}$ (AERONET)	$\eta_{R_F 440nm}$ (GRASP)	$\eta_{I_F 440nm}$ (GRASP)	$\eta_{R_C 440nm}$ (GRASP)	$\eta_{I_C 440nm}$ (GRASP)	$Reff_F$ (μm) (GRASP)	$Reff_C$ (μm) (GRASP)	SSA 440 nm (GRASP)
Saharan	05:58:32	05:58:32	Columnar	0.362	0.368 ± 0.009	0.224 ± 0.007	1.56	0.069	1.51	0.0004	0.178	2.526	0.913
Arabian	12:55:08	12:55:08	Columnar	0.306	0.291 ± 0.005	0.376 ± 0.0114	1.53	0.069	1.47	0.0001	0.153	2.512	0.887

Conclusions

Saharan and Middle East dominated cases were analyzed, utilizing Polly^{XT} Raman Lidar, sun-photometer and GRASP algorithm retrievals.

- ❖ The properties of size, sphericity, absorption and quantity of the desert dust cases in the atmospheric column and in layers are presented.
- ❖ From One- Step POLIPHON
  - One-step POLIPHON vertical profiles of Klett backscatter coefficient indicated the dominance of dust in the case of Saharan dust case and the mixture of dust and non-dust in the layer of Middle East dust (see plots 5b and 9b).
- ❖ Agreement GRASP algorithm parameters with AERONET
  - GRASP AOD at 440, 675, 870, 1020 nm **converges** with AERONET AOD at 440, 675, 870, 1020 nm (see plots 6a, 10a) indicating **good agreement**.
  - GRASP SSA at 440, 675, 870, 1020 nm mostly **does not converge** with AERONET AOD at 440, 675, 870, 1020 nm (see plots 6a, 10a), further analysis needed.
- ❖ Additional information from GRASP algorithm
  - For Saharan and Arabian dust layers SSA property showed that fine particles are strongly absorbing and coarse nearly all scattering.
  - The *columnar* η_{I_C} indicated non-absorbing coarse-mode particles and *columnar* η_{I_F} indicated strongly absorbing fine-mode particles for both studied cases. This is consistent with the SSA for coarse particles.
  - The vertical profile of extinction coefficients for the fine, coarse mode and total particles (see plots 5a, 9a). It revealed distinct particle mode dominance by aerosol type, characterizing the studied layers as follows: Saharan Dust - Coarse mode and Arabian Dust - Coarse mode. This highlights the importance on accurate layer aerosol classification.

***S:** Lidar ratio from Raman analysis. For 25/05/2025 analysis on 24/05/2025 at 18:00-20:00 at 0.8- 4 km and for 31/03/2024 analysis on 31/03/2024 at 20:00 - 22:30 at 0.8 – 2.8 km.

****δ:** Particle linear depolarization ratio; **S (sr):** Lidar ratio; **AOD:** Aerosol optical depth; **AE:** Angstrom Exponent; η_R: Real part of the refractive index; η_I: Imaginary part of the refractive index; **Reff:** Effective radius; **SSA:** Single Scattering Albedo; **F:** Fine-mode aerosols; **C:** Coarse-mode aerosols.

Acknowledgements: The study is supported by the 'EXCELSIOR': ERATOSTHENES: EXcellence Research Centre for Earth Surveillance and Space-Based Monitoring of the Environment H2020 Widespread Teaming project (www.excelsior2020.eu). The 'EXCELSIOR' project has received funding from the European Union's Horizon 2020 research and innovation programme under Grant Agreement No 857510, from the Government of the Republic of Cyprus through the Directorate General for the European Programmes, Coordination and Development and the Cyprus University of Technology. The authors acknowledge the ATARRI project funded by the European Union's Horizon Europe Twinning Call (HORIZON-WIDERA-2023-ACCESS-02) under the grant agreement No 101160258.